



Published in final edited form as:

J Biomol Screen. 2014 April ; 19(4): 497–507. doi:10.1177/1087057113516493.

Identification and optimization of PDE10A inhibitors using fragment-based screening by nanocalorimetry and X-ray crystallography

Michael I. Recht^{1,*}, Vandana Sridhar², John Badger², Pierre-Yves Bounaud², Cheyenne Logan², Barbara Chie-Leon², Vicki Nienaber², and Francisco E. Torres¹

¹Palo Alto Research Center, 3333 Coyote Hill Road, Palo Alto, CA 94304

²Zenobia Therapeutics, 3550 General Atomics Court, Building 2, Room 435, San Diego, CA 92121

Abstract

Fragment-based lead discovery (FBLD) is a technique in which, small, low-complexity chemical fragments of 6 to 15 heavy atoms are screened for binding to or inhibiting activity of the target. Hits are then linked and/or elaborated into tightly binding ligands, ideally yielding early lead compounds for drug discovery. Calorimetry provides a label-free method to assay binding and enzymatic activity that is unaffected by the spectroscopic properties of the sample. Conventional microcalorimetry is hampered by requiring large quantities of reagents and long measurement times. Nanocalorimeters can overcome these limitations of conventional isothermal titration calorimetry. Here we use enthalpy arrays, which are arrays of nanocalorimeters, to perform an enzyme activity-based fragment screen for competitive inhibitors of phosphodiesterase 10A (PDE10A). Two dozen fragments with $K_I < 2$ mM were identified and moved to crystal soaking trials. All soak experiments yielded high resolution diffraction with two-thirds of the fragments yielding high-resolution co-crystal structures with PDE10A. The structural information was used to elaborate fragment hits, yielding leads with $K_I < 1$ μ M. This study shows how array calorimetry can be used as a prescreening method for fragment-based lead discovery with enzyme targets and paired successfully with an x-ray crystallography secondary screen.

Keywords

nanocalorimetry; enzyme assay; label-free assay; fragment-based lead discovery; X-ray crystallography

Introduction

Modulation of the cyclic nucleotide phosphodiesterase (PDE) class of enzymes has provided drugs for the treatment of heart failure, chronic obstructive pulmonary disease (COPD),

*Corresponding author: michael.recht@parc.com, Tel: 650-812-4843, FAX: 650-812-4251.

Conflict of interest statement

M. Recht and F. Torres are employed by Palo Alto Research Center Incorporated. All other authors are employed by Zenobia Therapeutics.

erectile dysfunction, and pulmonary hypertension¹. Phosphodiesterases consist of 11 families (PDE1 through PDE11) and are classified by the substrate (cAMP and/or cGMP) that they hydrolyze. There are more than 60 isoforms of phosphodiesterases either encoded by distinct genes or resulting from splice variants from individual genes.

Phosphodiesterase 10A (PDE10A) is expressed at high levels in the striatal medium spiny neurons²⁻⁴ where it regulates both cAMP and cGMP signaling cascades making it an attractive target for correcting the misregulation of cAMP signaling^{5, 6}. Reduction of PDE10A mRNA and protein levels in striatum of transgenic mice implies a role of PDE10A in Huntington's disease (HD). This hypothesis has been recently tested in a well-established transgenic mouse model of HD (R6/2)⁷. The selective PDE10 inhibitor, TP-10, was administered intraperitoneally (IP) to R6/2 mice beginning at 4 weeks of age and resulted in amelioration of a number of neurological and behavioral measures of brain damage and a decrease in striatal and cortical cell loss. Specific results included a delay of onset of abnormal hind-limb clasping response and improvement of balance on an accelerating rotarod. TP-10 reduced by 50% the loss of striatal size and decreased the number of intranuclear inclusions of aggregated mhtt. The PDE10 inhibitor papaverine has efficacy in attenuating some cognitive deficits observed in schizophrenia, and therefore inhibition of PDE10 may represent an approach to treatment of psychosis^{6, 8}.

Fragment-based lead discovery (FBLD) is a technique in which, small, low-complexity chemical fragments of 6 to 15 heavy atoms are screened for binding to or inhibiting activity of the target. Hits are then linked and/ or elaborated into tightly binding ligands, ideally yielding early lead compounds for drug discovery⁹⁻¹¹.

Treatment of central nervous system (CNS) disorders requires that compounds penetrate the CNS by crossing the blood brain barrier (BBB), which can be challenging to achieve starting with high molecular weight initial hits. For CNS disease, FBLD has advantages over more typical high-throughput screening (HTS) for targeted discovery because in general it has been shown to yield lower molecular weight clinical candidates and has the added benefit that other chemical properties consistent with CNS penetration may be engineered during the optimization process¹².

Previously, we used a calorimetric enzyme activity assay to identify several fragment inhibitors of the cAMP-specific phosphodiesterase PDE4A¹³. We were unable to obtain high-quality structure data with any of the fragment hits and did therefore not perform any elaboration of these hits to obtain more potent inhibitors. Here we have combined a calorimetric enzyme activity assay and X-ray crystallographic structure data to obtain more than two dozen fragment inhibitors of PDE10A with two thirds yielding high-resolution co-crystal structures appropriate for further structure-directed drug design. In addition, we describe the elaboration of selected fragment hits into sub-micromolar inhibitors.

Materials & Methods

PDE10A Cloning, Expression, and Purification

The catalytic domain of PDE10A2 (EC 3.1.4.17) was expressed and purified as described by Wang et al.¹⁴ with modification.

PDE10A was cloned into a proprietary vector containing an N-terminal 6Xhis tag, cleavable by TEV protease. Positively identified clones were expressed in BL21(DE3) RIL cells. Cells containing target plasmid were grown in LB containing selection antibiotics at 37 °C until OD 600=0.7–0.8. Cells were induced with 0.1 mM isopropyl- β -D-thiogalactopyranoside (IPTG) at 15 °C overnight. The cells were harvested and stored at –80 °C. Cell pellets were lysed in 50 mM Tris (pH 8.0), 500 mM NaCl, 0.1% (w/v) NP-40, and 10 mM imidazole (lysis buffer) containing one Roche Complete Protease Inhibitor Tablet and 20,000 units of Benzonase. The suspension was sonicated on ice for 2 min at 70% output with a 25% duty cycle. Clarified supernatant was loaded onto Ni²⁺-charged IMAC. Peak fractions containing target protein were cleaved overnight with TEV protease. Cleaved protein was isolated by running the sample over Ni²⁺ charged IMAC, collecting flow-through. Protein was characterized for relative oligomeric state by size exclusion chromatography in 20 mM HEPES (pH 7.5), 150 mM NaCl, and 5 mM dithiothreitol (DTT). Monomeric PDE10A was concentrated to 12 mg/mL for crystallization.

Fragment Library

Select compounds from commercial fragment libraries, Zenobia Therapeutics Library 1 and Library 2 (Zenobia Therapeutics, San Diego, CA) were used in this study. For the initial screen, we used fresh solutions of individual compounds dissolved at 200 mM in DMSO. The average molecular weight of the compounds was 153, and the average number of heavy atoms was 10.7.

PDE10A Calorimetric Activity Assay

Enthalpy arrays are arrays of nanocalorimeters that allow scientists to measure thermodynamics and kinetics of molecular interactions using small sample volumes (250 nL) and short measurement times (typically 5–10 min)¹⁵. Previously, we demonstrated the use of enthalpy arrays in FBLD to identify fragment inhibitors of PDE4A¹³.

For enthalpy array screening of fragments, hydrolysis of 3',5'-cGMP was measured at 21 °C in 100 mM Tris-HCl (pH 7.5), 10 mM MgCl₂, 1 mM tris(2-carboxyethyl) phosphine (TCEP), and 2% (v/v) DMSO. Each enthalpy array detector contains a sample region and a reference region, which are designated based on the material deposited on the region (see Fig. 1 of Recht et al. 2009;¹⁶). The sample region materials consisted of a drop of PDE10A (30 μ M) and a drop of substrate solution (4 mM 3',5'-cGMP). The reference region used a drop of buffer and a drop of the same substrate solution (4 mM 3',5'-cGMP) used in the sample region. The combined drops in the sample region contained 15 μ M PDE10A and 2.0 mM 3',5'-cGMP, and the combined drops in the reference region contained 2.0 mM 3',5'-cGMP. Reactions with compounds from the fragment library (2 mM in the combined drops, except as noted) were performed as above, except that a single compound (4 mM, except as

noted) was included with the substrate (4 mM 3',5'-cGMP). Guanosine 3',5'-cyclic monophosphate, adenosine 3',5'-cyclic monophosphate, pentoxifylline, papaverine hydrochloride, and 3-isobutyl-1-methylxanthine (IBMX) were obtained from Sigma-Aldrich (St. Louis, MO) and used without further purification. The concentration of the 3',5'-cGMP stock solution (adjusted to pH 7 with dilute NaOH) was determined by measuring the absorbance at 254 nm and using an extinction coefficient of $13000 \text{ M}^{-1} \text{ cm}^{-1}$ ¹⁷.

We used an enzyme concentration that would result in a good signal-to-noise ratio at V_{max} , and the substrate concentration was then adjusted to produce the length of reaction desired. Typically, three replicates of each measurement were performed, and the average and standard error of the mean of the measurements are reported. Measurements with inhibitors had a corresponding set of control measurements without inhibitor performed at the side by side.

PDE10A shows dual activity, so hydrolysis of either 3',5'-cAMP or 3',5'-cGMP could be monitored. To reduce the amount of enzyme used in the screen, we used 3',5'-cGMP as the substrate because PDE10A has a higher k_{cat} with this substrate.

Microcalorimetric enzyme assays were performed using an iTC200 (Microcal/GE Healthcare). Hydrolysis of 3',5'-cGMP was measured at 25 °C in 100 mM Tris-HCl (pH 7.5), 10 mM MgCl_2 , 1 mM tris(2-carboxyethyl) phosphine (TCEP), and 2% (v/v) DMSO. The sample cell (200 μL) contained PDE10A (100 nM) the injection syringe contained 4 mM 3',5'-cGMP. Ten microliters of 4 mM 3',5'-cGMP was injected in the sample cell to initiate the reaction.

Data Analysis

Data analysis of enthalpy array and microcalorimetric reactions was performed as described in Recht et al, 2012¹³.

Protein Crystallization, Data Collection, and Structure Determination

Apo crystals for soaking experiments were grown by the hanging drop vapor diffusion method from a well solution of 18% PEG 4450, 0.2 M calcium acetate and 50mM BME. Crystals were cryo-protected using well solution plus 25% ethylene glycol. Compounds were prepared for soaking as a 100mM stock in 100% DMSO and diluted to a final concentration of 2.5mM using well solution. Crystals were soaked overnight by adding 4 μL of compound stock to 4 μL of well solution containing the crystal. The final concentration of compound in these experiments was 1.25mM.

Data sets collected from crystals soaked with small fragment compounds were measured at the Advanced Photon Source at Argonne National Labs (Chicago, IL) on beamlines 22ID (Mar 300 detector), 22BM (Mar 225 detector) and at the Canadian Light Source on beamline 21ID-D (Rayonix 300 detector). All of the crystals used in these experiments diffracted to at least 2.0 Å resolution. The data sets obtained from crystals containing the small fragment compounds ZT0143 and ZT0451 were collected on a rotating anode x-ray source with a Mar 345 detector at the UCSD Biomolecule Crystallography facility to somewhat lower resolution (2.3 Å). The two crystals that contained the elaborated compounds ZT1595 and

ZT1597 diffracted to medium resolution (2.5–2.8 Å) at the Canadian Light Source on beamline 21ID-D. All data sets measured at synchrotron sources were integrated and merged with the HKL2000 software¹⁸. The two data sets collected at the UCSD laboratory source were integrated with MOSFLM¹⁹ and merged with SCALA²⁰. Structure solution calculations was initiated by molecular replacement with MOLREP²¹ using a search model developed from PDB entry 2OUR¹⁴ and models were refined with the program REFMAC²². Structures were initially refined without solvent and then refined subject to a limited water-picking protocol. Using this automated protocol, the resulting models were sufficiently well refined to calculate initial, unbiased electron density maps for the visual assessment of compound binding. All of the soaked crystals and protein conformations were highly isomorphous to the apo crystals (space group $P2_12_12_1$ $a=50.6$, $b=50.6$, $c=155.7$) and are very similar to a previously solved crystal form [13]. The models associated with the data sets that revealed bound fragments were finalized with additional cycles of model-building and refinement (Supplemental Table S1). Changes made to the models during these cycles included the fitting of bound fragment compounds, additional water picking, minor adjustments to the protein conformation and the incorporation of discrete disorder in selected side chains. Fragments were visualized in molecule A but not molecule B as observed by Wang et al., 2007¹⁴. Lack of binding at molecule B is most likely due to an alternate conformation of helix H14 and the M-loop that partially blocks the active site (see¹⁴).

Fragment optimization

Chemical synthesis of elaborated fragments was done at Peptech Corporation (Bedford, MA). Synthetic details and compound characterization can be found in the Supplementary Material.

Results

The calorimetric activity assay was validated using three known general phosphodiesterase inhibitors and a PDE10A specific inhibitor: IBMX, pentoxifylline, and papaverine (Table 1 and Supplemental Figure S1). All inhibitors display competitive inhibition of PDE10A, with K_I values in reasonable agreement with those expected based on IC_{50} values in the literature (Table 1; IBMX $IC_{50}= 11 \mu\text{M}$;²³; papaverine hydrochloride $IC_{50}= 95 \text{ nM}$;²⁴).

Previously, we had used the enthalpy array technology to identify inhibitors of the 3',5'-cAMP specific phosphodiesterase, PDE4A¹³. We tested these inhibitors against PDE10A and the results are shown in Figure 1A and summarized in Table 1. All the fragments that showed activity against PDE4A also inhibited PDE10A with ligand efficiencies greater than or equal to 0.30. Five of the compounds showed significantly higher potency against PDE10A than PDE4A. Fragment ZT0450, which showed mixed inhibition against PDE4A, showed only competitive inhibition against PDE10A. In contrast to the increase in K_M and reduction in k_{cat} observed with ZT0450 and PDE4A, only an increase in K_M was observed with PDE10A at the highest concentration of ZT0450 tested (2 mM). It is possible that the differences in the substrate contact pattern and the overall shape and size of the substrate

binding pocket of these two phosphodiesterases^{14, 25} contribute to the different observed inhibition mechanisms.

The activity-based enthalpy array screen with the catalytic domain of PDE10A against an 85-compound fragment library was performed at a compound concentration of 2 mM. Corresponding control reactions in the absence of any inhibitor were performed for every five fragments tested and acted as the basis for comparison of K_M values for those five fragments. Figure 1B displays the results of the fragment screen as the ratio of the K_M in the presence of fragment ($K_{M, app}$) to the K_M of the corresponding control reaction ($K_{M, control}$). Seven compounds produced a K_M ratio ≥ 2 . These were considered hits, and 6 of 7 were confirmed to have $K_I \leq 2$ mM using fresh stocks of fragments and protein and testing using the microcalorimetry assay. The one compound that did not have $K_I < 2$ mM upon retesting (ZT0826) also had a ligand efficiency lower than 0.3. The K_I and ligand efficiencies for all compounds that produced a K_M ratio greater than 2 are presented in Table 2.

There was one compound (ZT0401) that produced highly sticky drops on the surface of the enthalpy array, making quantitative analysis of the inhibition data difficult. This compound was tested using the microcalorimeter-based enzymatic assay, yielding the K_I and LE data shown in Table 2.

All eight inhibitors identified in the PDE10A screen as well as the 16 previously identified PDE4A hits were moved into X-ray crystallography studies. As we were able to obtain high-quality apo-PDE10A crystals, soaking experiments were performed and yielded complexes in 16 out of 24 cases (66.7%) at the ligand concentration tested (1.25 mM). We obtained co-crystal structures with 4 of the 8 PDE10A inhibitors (50%) and with 12 of the 16 (75%) previously identified PDE4A inhibitors (Tables 1 and 2). We did not attempt additional soaking experiments at higher ligand concentration as this resulted in crystal cracking.

Figure 2 shows a superposition of all the co-crystal structures of fragments bound to PDE10A. All of the fragments bind in the primary binding pocket in PDE10A sandwiched between Phe 729 on one side and Ile692 and Phe696 on the other. Some compounds have hydrogen bond donors or acceptors within standard hydrogen bonding distance of Gln 726. No additional binding sites were identified using our protocol.

For PDE10A, a second “specificity” pocket at the active site has been identified²⁶ and compounds that occupy this site have been shown to be specific for PDE10A over other PDEs¹. PDE10A has a unique glycine residue (725) that is typically a larger side chain that blocks this site in other PDEs.

We selected two fragment hits (ZT0143 and ZT0451) to optimize to occupy the specificity site based upon the x-ray structure of the PDE10A complex. To ensure specificity and minimize added molecular weight, we focused on improving the potency of our fragments by growing into the specificity site first. These fragments were selected because they were of reasonable starting potency (~ 100 μ M), ligand efficiency (>0.4) and had functional groups for chemical modification directed towards the specificity pocket as revealed by their x-ray crystal structures.

Figures 3A and B show the crystal structures of the fragment hit ZT0143 and an optimized compound (ZT1597; PDB ID 4MSE) obtained by growing the fragment into the specificity pocket. The N3 and 2-amino groups of ZT0143 are within standard hydrogen bonding distance to Gln726. The optimized compound has a 2-amino to 2-methyl substitution compared to the original fragment hit which appears to be tolerated in the binding pocket as evidenced by the equal potency of compound ZT1608 compared to the original fragment (Figure 3C). The benzothiazole core of the optimized compound rotates compared to the fragment (Figure 3B), moving the N3 beyond standard hydrogen bonding distance to Gln726 but placing the nitrogen of the quinoline moiety within standard hydrogen bonding distance of Tyr693 in the specificity pocket. The single substitution in the specificity pocket leads to a 100-fold improvement in potency. Substituting at either the 4 or the 5 position while maintaining the 2-amino group (ZT1752, ZT1694) did not lead to improved potency compared to the optimized compound (Figure 3C).

Crystal structures and optimization of fragment ZT0451 are shown in Figure 4. The N1 of ZT0451 is within standard hydrogen bonding distance to the side chain of Gln 726 and the 8-nitro group may also make a long hydrogen bond with Gln 726. The optimized compound (ZT1595; PDB ID 4MSC) is substituted at the 7-position and the quinoline core rotates compared to the original fragment. This rotation places the N1 of the quinoline core beyond standard hydrogen bonding distance to Gln726 but places the nitrogen of the second quinoline within standard hydrogen bonding distance of Tyr693 in the specificity pocket. Again, the single substitution in the specificity pockets yields an approximately 100-fold increase in potency compared to the fragment hit. Substitutions at either the 8-position (ZT1638, ZT1525) or the 7-position (ZT1595, ZT1598) yield compounds with similar potency (Figure 4B). In all cases, the optimized compounds showed competitive inhibition of PDE10A.

Both optimized fragments (ZT1597 and ZT1595) show specificity for PDE10A, having at least 10-fold more potency against PDE10A than PDE4A (Figures 4 and 5). Neither compound inhibited PDE4A at the highest concentration tested but, due to solubility limits of the optimized fragments, the K_I against PDE4A could not be determined.

Discussion

We observed that two-thirds of the calorimetrically identified fragment hits yielded X-ray structures. Compared to reports in literature using other techniques (SPR, NMR and fluorescence)^{27, 28}, this is a higher proportion of fragment hits yielding X-ray structures. There are several possible explanations for the high proportion of crystallizable fragment hits seen here. First, the compounds in the library have high aqueous solubility, allowing them to be screened at high concentration in the activity assay with 2% residual DMSO and to be soaked at high concentration into the apo protein crystals. Our cutoff for defining a hit is a $K_I < 2$ mM and a $LE > 0.3$, which selects for relatively potent fragments that are active at a concentration well below their solubility limit. Other researchers will try to crystallize hits with K_d over 10 mM and LE lower than 0.3, which may result in solubility limitations being an issue during crystallization trials. Second, the hits act as competitive inhibitors, ensuring that they bind in the substrate binding pocket which is accessible in the apo protein crystals.

Additionally, selecting only competitive inhibitors means that the compounds are unlikely to be aggregators (promiscuous inhibitors)²⁹, and thus provides a way to minimize the number of hits that are non-drug-like “nuisance” compounds. Finally, the identity of the protein target is a factor. We obtained high quality crystals of the apo form of the protein into which fragments could be soaked, which is not always the case. For example, we were unable to obtain X-ray structures of any fragment hits bound to PDE4A¹³ even though we obtained crystals with 75% of the PDE4A active fragments in complex with PDE10A.

Fragments that crystallized had a higher potency on average ($K_I = 590 \pm 94 \mu\text{M}$) than those that did not ($K_I = 1000 \pm 140 \mu\text{M}$; $p = 0.018$). Although the p -value indicates significance in K_I 's of fragments found in crystals compared to those that did not crystallize, using of threshold to decide which fragments to crystallize is not ideal. For example, using a threshold of $870 \mu\text{M}$ (average plus 3 sigma) would yield 3 false positives (from total of 8 true negatives) and 5 false negatives (from total of 16 true positives). Consistent with our observation here, Wielens et al (2013)²⁸ report obtaining crystal structures with fragments that “appear to be generally more potent”.

Comparison of other properties of the fragments (LE, calculated logP (clogP), ligand lipophilicity efficiency (LLE), and polar surface area (PSA)) did not yield any statistically significant differences between those that crystallized and those that did not. Therefore, we would favor trying to crystallize all confirmed fragment hits from the activity-based calorimetric assay rather than setting another threshold for moving forward to crystallization trials.

With the availability of X-ray structures of complexes, optimization of fragments can be performed by synthesizing specific structure-based modifications. These modifications include growing the fragment into potential binding pockets (as we have done here) or linking two fragments that bind to non-overlapping sites in the target¹⁰. Elaboration of fragment hits into specificity pockets yielded increased potency and specificity for PDE10A over PDE4A (Figures 4 and 5). Having access to X-ray structures during the optimization process proved essential as elaborated fragments can move within the binding pocket to find a better fit, compared to the original fragment. In this particular case, reaching into the PDE10-specificity pocket overall achieved a lower energy minimum than interacting with the Gln726 residue, thus reorienting the original scaffold as seen with ZT1595 and ZT1597. Such movements would be hard to predict from structure-activity relationships (SAR) alone. The X-ray structures of ZT1595 and ZT1597 provide new vectors for further synthetic developments, for example targeting the back of the binding pocket by coming off the methyl group of ZT1597.

For initial screening, enthalpy arrays can be used to identify hits with inhibition constants as low as 2 nM, but the technique is not well-suited to characterization of potent inhibitors. As previously observed, the lower limit for which K_I can be reliably determined is 1/50th of the enzyme concentration¹⁶. For assays with PDE10A, which was present at $15 \mu\text{M}$ in the final reactions, the limit on accurate determination of K_I is 300 nM. As it is unlikely that a fragment will bind with this level of potency, the enthalpy array method is ideal for the initial fragment screen. More potent compounds may be tested using a conventional

microcalorimeter. The lower enzyme concentration (100 nM) used in these assays still yields good signal-to-noise and extends the limit of K_I determination down to the single digit nanomolar range. Alternatively, for this level of potency, more conventional activity assays are accurate and would most likely be used at this point of the discovery program.

In principle, one could perform an activity-based fragment screen using an automated conventional microcalorimeter such as the MicroCal Auto iTC200. The advantage of this technique over the enthalpy arrays is the higher sensitivity and ability to accurately measure K_I over a broader range (~10 nM to ~2 mM for microcalorimetry compared to ~500 nM to ~2mM for the enthalpy array)³⁰. The tradeoff of using a lower enzyme concentration is that it takes about 30 minutes to run each reaction, limiting the throughput to a little over 20 compounds per day. One could increase the throughput by raising the enzyme concentration by a factor of 2–3, but this solution has two limitations: first, for substrates with K_M values below 1 μ M (like 3',5'-cAMP with PDE10A), one loses the ability to measure K_M (and therefore K_I of competitive inhibitors) with high accuracy because the rate at which the reaction decays as the substrate concentration drops below the K_M occurs on a time scale that is fast compared to the instrument response time (~10 sec). Second, the maximum differential power signal ($P = H \cdot k_{cat} \cdot [E] \cdot \text{volume}$) that can be recorded (12 μ cal/s) may be exceeded by have the reaction occur at too high a rate. For initial screening smaller libraries of a few hundred compounds, Auto iTC200 would be a viable option.

Using calorimetry to prescreen fragments for inhibition of enzymatic activity has several benefits: First, only 10% of the fragments showed inhibition and were subsequently fed into the X-ray crystallographic secondary screen. This significantly reduced the number of structural characterizations, resulting in savings in labor and material costs. Second, the prescreening data shows which compounds have an effect on the activity of the enzyme and their inhibition mechanism, indicating that a fragment is binding to a site of functional interest rather than simply binding. Finally, because calorimetry is a label-free technique, the assay is resistant to compound interference that can occur with fluorescence or absorbance based enzymatic activity assays. When combined with a structural technique, such as X-ray crystallography, calorimetry is an effective method to improve the efficiency of fragment-based drug discovery for enzyme targets.

Supplementary Material

Refer to Web version on PubMed Central for supplementary material.

Acknowledgments

This work was supported by grant R01EB009191 from the National Institute of Biomedical Imaging and Bioengineering, National Institutes of Health (NIH). Its contents are solely the responsibility of the authors and do not necessarily represent the official views of the NIH. We thank Rick Walter and Gina Ranieri (Shamrock Structures) for data collection at the Advanced Photon Source and the Canadian Light Source. We thank Nicholas Nguyen for assistance with equipment at the UCSD Biomolecule Crystallography Facility.

References

1. Chappie TA, et al. Current landscape of phosphodiesterase 10A (PDE10A) inhibition. *J Med Chem.* 2012; 55(17):7299–7331. [PubMed: 22834877]

2. Coskran TM, et al. Immunohistochemical localization of phosphodiesterase 10A in multiple mammalian species. *J Histochem Cytochem.* 2006; 54(11):1205–1213. [PubMed: 16864896]
3. Seeger TF, et al. Immunohistochemical localization of PDE10A in the rat brain. *Brain Res.* 2003; 985(2):113–126. [PubMed: 12967715]
4. Xie Z, et al. Cellular and subcellular localization of PDE10A, a striatum-enriched phosphodiesterase. *Neuroscience.* 2006; 139(2):597–607. [PubMed: 16483723]
5. Schmidt CJ, et al. Preclinical characterization of selective phosphodiesterase 10A inhibitors: a new therapeutic approach to the treatment of schizophrenia. *J Pharmacol Exp Ther.* 2008; 325(2):681–690. [PubMed: 18287214]
6. Siuciak JA, et al. Inhibition of the striatum-enriched phosphodiesterase PDE10A: a novel approach to the treatment of psychosis. *Neuropharmacology.* 2006; 51(2):386–396. [PubMed: 16780899]
7. Giampa C, et al. Inhibition of the striatal specific phosphodiesterase PDE10A ameliorates striatal and cortical pathology in R6/2 mouse model of Huntington's disease. *PLoS One.* 2010; 5(10):e13417. [PubMed: 20976216]
8. Rodefer JS, et al. PDE10A inhibition reverses subchronic PCP-induced deficits in attentional set-shifting in rats. *Eur J Neurosci.* 2005; 21(4):1070–1076. [PubMed: 15787711]
9. Carr RA, et al. Fragment-based lead discovery: leads by design. *Drug Discov. Today.* 2005; 10(14):987–992. [PubMed: 16023057]
10. Erlanson DA, et al. Fragment-based drug discovery. *J. Med. Chem.* 2004; 47(14):3463–3482. [PubMed: 15214773]
11. Jahnke, W.; Erlanson, DA. *Fragment-based approaches in drug discovery.* Wiley-VCH; 2006. p. xxiip. 369[Chichester : John Wiley, distributor]: Weinheim
12. Nienaber V. Start small and stay small. Minimizing attrition in the clinic with a focus on CNS therapeutics. *Curr Top Med Chem.* 2009; 9(18):1688–1704. [PubMed: 19929834]
13. Recht MI, et al. Fragment-based screening for inhibitors of PDE4A using enthalpy arrays and X-ray crystallography. *J Biomol Screen.* 2012; 17(4):469–480. [PubMed: 22223051]
14. Wang H, et al. Structural insight into substrate specificity of phosphodiesterase 10. *Proc. Natl. Acad. Sci. U. S. A.* 2007; 104(14):5782–5787. [PubMed: 17389385]
15. Torres FE, et al. Enthalpy arrays. *Proc. Natl. Acad. Sci. U.S.A.* 2004; 101(26):9517–9522. [PubMed: 15210951]
16. Recht MI, et al. Measurement of enzyme kinetics and inhibitor constants using enthalpy arrays. *Anal. Biochem.* 2009; 388:204–212. [PubMed: 19250916]
17. O'Neil, MJ. *The Merck index : an encyclopedia of chemicals, drugs, and biologicals.* 14th ed.. Whitehouse Station, N.J.: Merck; 2006.
18. Otwinowski Z, Minor W. Processing of X-ray diffraction data collected in oscillation mode. *Methods Enzymol.* 1997; 276:307–326.
19. Leslie AG. The integration of macromolecular diffraction data. *Acta crystallographica. Section D, Biological crystallography.* 2006; 62(Pt 1):48–57.
20. Evans P. Scaling and assessment of data quality. *Acta crystallographica. Section D, Biological crystallography.* 2006; 62(Pt 1):72–82.
21. Vagin A, Teplyakov A. Molecular replacement with MOLREP. *Acta crystallographica. Section D, Biological crystallography.* 2010; 66(Pt 1):22–25.
22. Murshudov GN, et al. Refinement of macromolecular structures by the maximum-likelihood method. *Acta crystallographica. Section D, Biological crystallography.* 1997; 53(Pt 3):240–255.
23. Fujishige K, et al. Striatum- and testis-specific phosphodiesterase PDE10A isolation and characterization of a rat PDE10A. *Eur J Biochem.* 1999; 266(3):1118–1127. [PubMed: 10583409]
24. Grauer SM, et al. Phosphodiesterase 10A inhibitor activity in preclinical models of the positive, cognitive, and negative symptoms of schizophrenia. *J Pharmacol Exp Ther.* 2009; 331(2):574–590. [PubMed: 19661377]
25. Wang H, et al. The molecular basis for different recognition of substrates by phosphodiesterase families 4 and 10. *J. Mol. Biol.* 2007; 371(2):302–307. [PubMed: 17582435]
26. Verhoest PR, et al. Discovery of a novel class of phosphodiesterase 10A inhibitors and identification of clinical candidate 2-[4-(1-methyl-4-pyridin-4-yl)-1H-pyrazol-3-yl]-

- phenoxymethyl]-quinoline (PF-2545920) for the treatment of schizophrenia. *J Med Chem.* 2009; 52(16):5188–5196. [PubMed: 19630403]
27. Pollack SJ, et al. A comparative study of fragment screening methods on the p38alpha kinase: new methods, new insights. *J Comput Aided Mol Des.* 2011; 25(7):677–687. [PubMed: 21732248]
 28. Wielens J, et al. Parallel screening of low molecular weight fragment libraries: do differences in methodology affect hit identification? *J Biomol Screen.* 2013; 18(2):147–159. [PubMed: 23139382]
 29. Shoichet BK. Screening in a spirit haunted world. *Drug Discov Today.* 2006; 11(13–14):607–615. [PubMed: 16793529]
 30. Torres FE, et al. Higher throughput calorimetry: opportunities, approaches and challenges. *Curr Opin Struct Biol.* 2010; 20(5):598–605. [PubMed: 20888754]

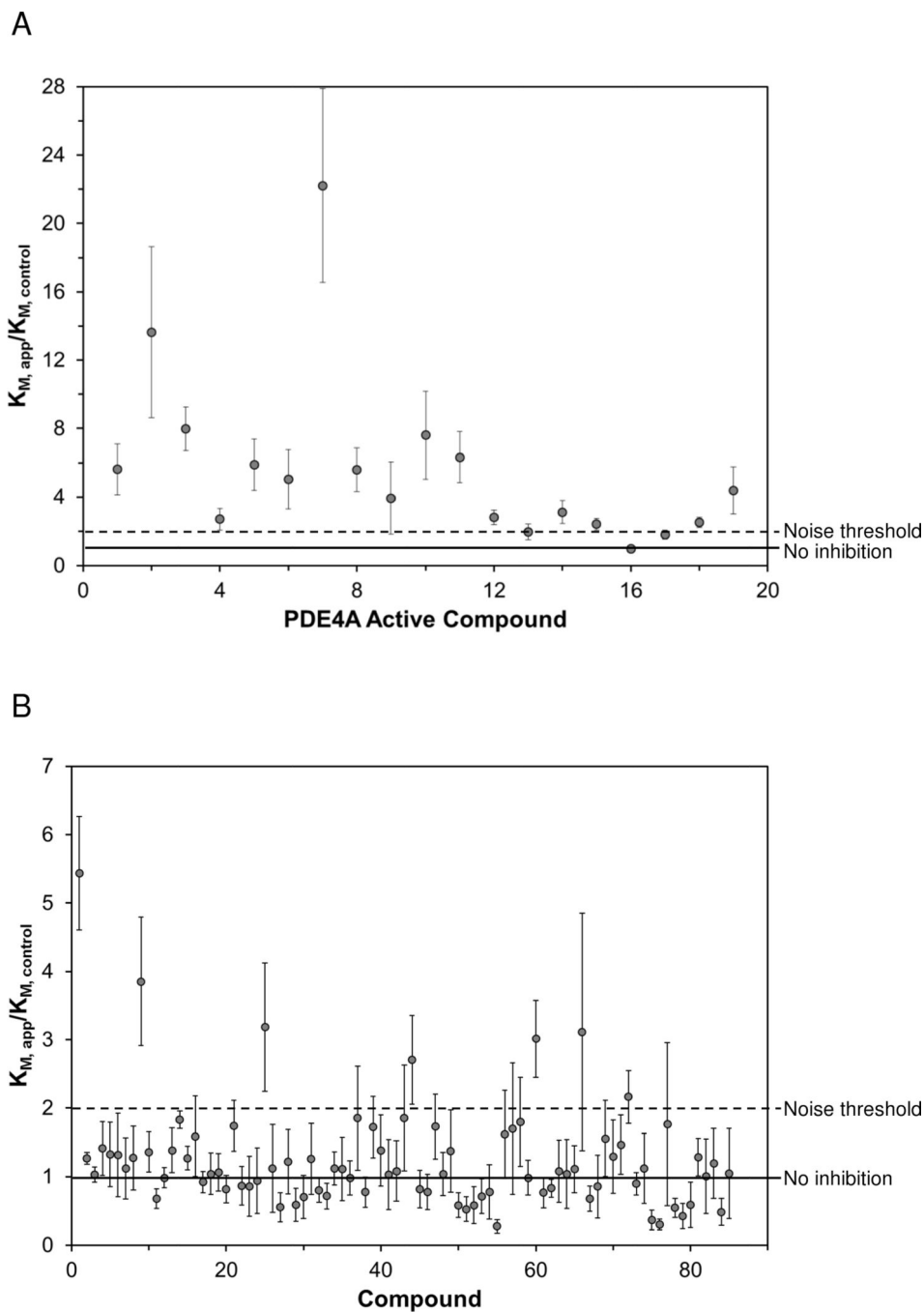


Figure 1.

Results of the fragment screen for inhibitors of PDE10A using the calorimetric activity assay. The ratio of the K_M in the presence of the fragment ($K_{M, app}$) to the K_M of an associated control reaction ($K_{M, control}$) is shown. Compounds were tested at 2 mM concentration. For every five compounds, an associated control reaction (no inhibitor) was run and served as the $K_{M, control}$ for those compounds. The solid line indicates a K_M ratio of 1, which means no effect compared to control. The dashed line indicates a K_M ratio of 2, the noise threshold selected for a compound to be classified as a hit. The error bars indicate the standard error of the mean for the K_M ratio. (A) Previously identified PDE4A inhibitors, (B) 85 compound fragment library.

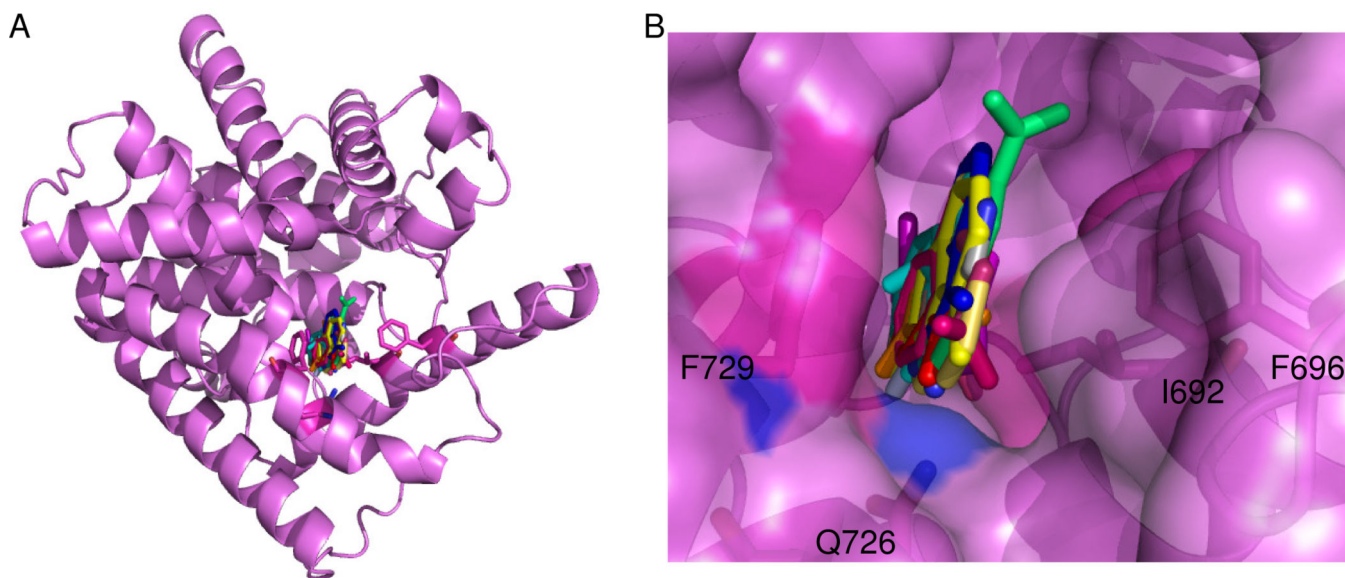
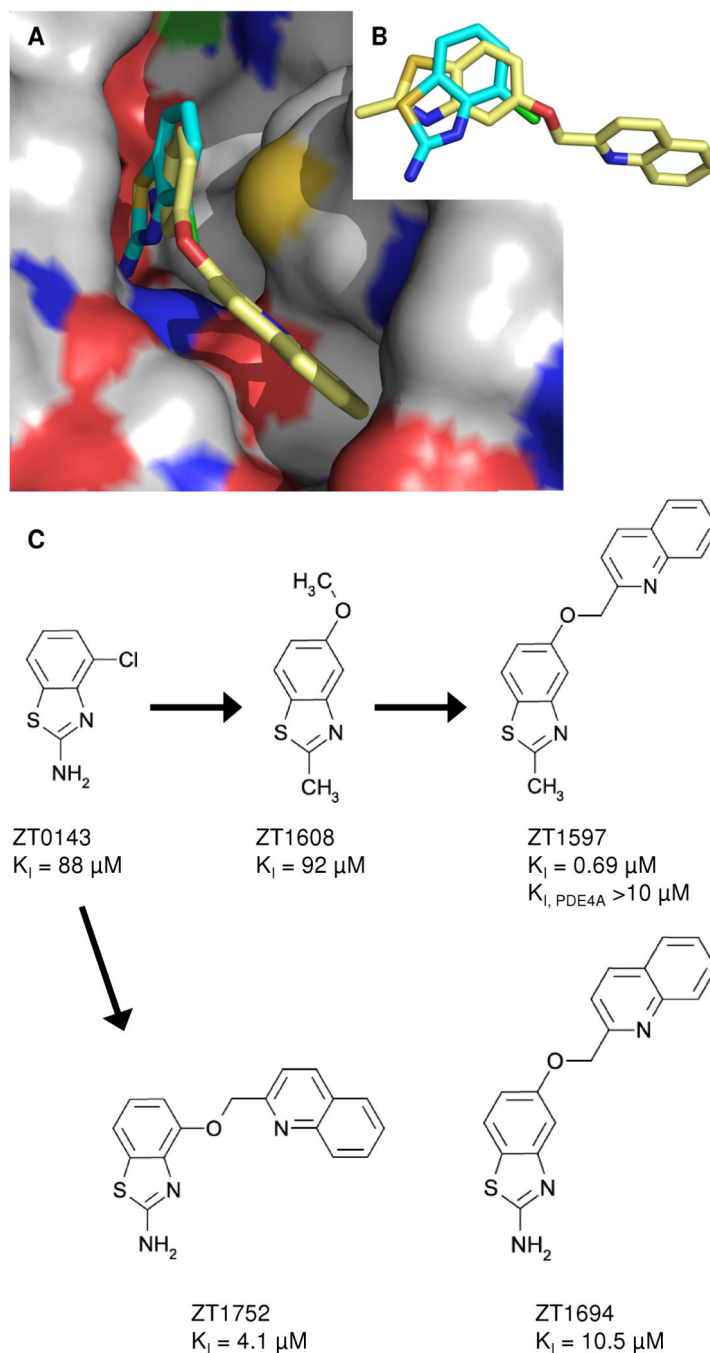


Figure 2.

(A) Location of fragments binding to PDE10A in this study. All fragments were found at the primary binding pocket typically occupied by cAMP or cGMP¹⁴. Fragments were not located at any other binding site on the protein. (B) Close-up of a superposition of all co-crystal structures of fragments bound in the primary binding pocket of PDE10A. Fragments are found along a single plane and oriented between F729 and I692, F696. Q726 is making at least one hydrogen bond with all of the fragment hits.

**Figure 3.**

Crystal structures for key compounds derived from fragment ZT0143. (A) Overlay of ZT0143 (cyan) and ZT1597 (yellow) showing binding at the specificity pocket for the optimized fragment. (B) Fragment core rotates in ZT1597 versus ZT0143 such that the substituent is pointed towards the specificity pocket. (C) Optimization path for ZT0143.

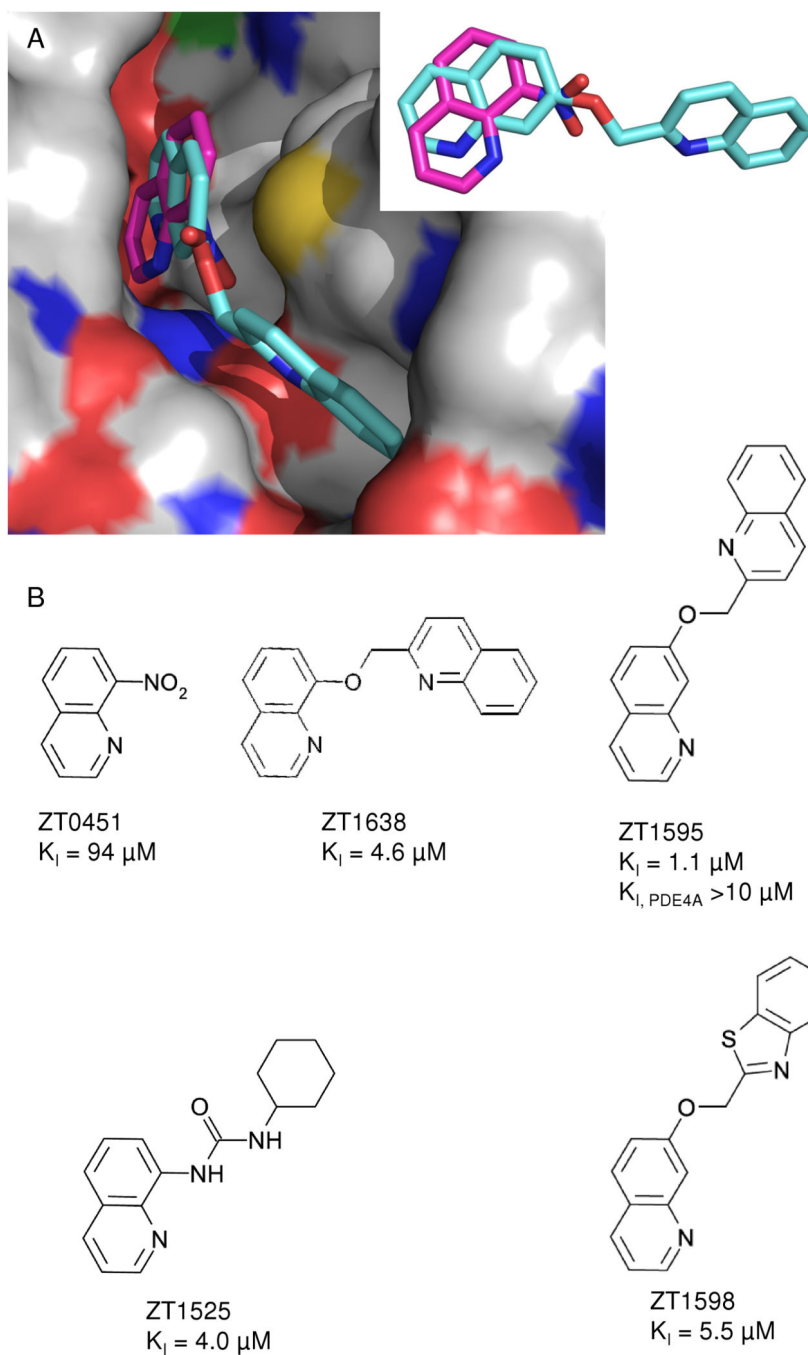
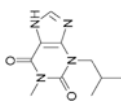
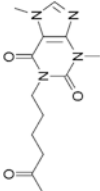
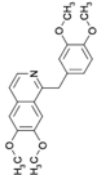
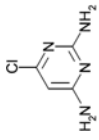
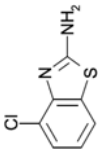
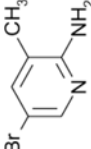
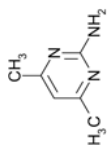
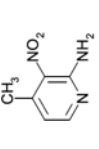
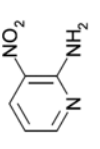
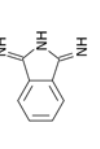
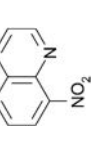
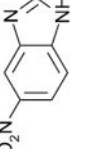
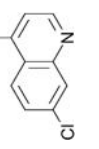
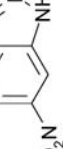


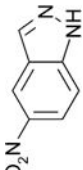
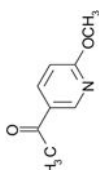
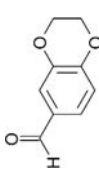
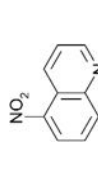
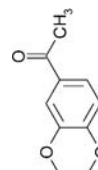
Figure 4.

Crystal structures for key compounds derived from ZT0451. (A) X-ray structures of ZT0451 (magenta) and ZT1595 (cyan). Inset showing a rotation of the core to accommodate the R-group at the specificity pocket. (B) Original fragment hit ZT0451 and modifications at the nitro-group which is pointing towards the specificity pocket in PDE10. Four analogues showing significant increase in potency are summarized.

Table 1
Inhibition Constants and Ligand Efficiencies of Compounds Sorted Based on Ligand Efficiency.

Compound	Structure	Ligand Efficiency (kcal mol ⁻¹ HA ⁻¹) PDE10A	K _i (μM), PDE10A	K _i (μM), PDE4A	X-ray; PDB ID
Control inhibitors					
IBMX (a)		0.41	17 ± 6.6	8.3 ± 1.5	NA
Pentoxifylline (c)		0.25	200 ± 60	72 ± 18	NA
Papaverine (d)		0.33	1.0 ± 0.14	NA	NA
Fragments					
ZT0443 (5)		0.51	410 ± 100	1400 ± 140	Y; 4MSO
ZT0143 (b) (2)		0.45	210 ± 76	580 ± 72	Y; 4MSH
ZT0431 (12)		0.44	1100 ± 170	2000 ± 300	N

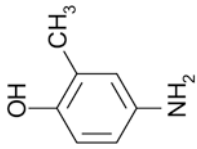
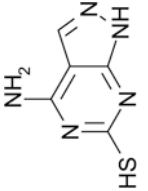
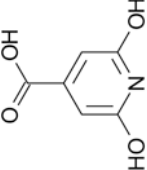
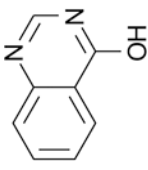
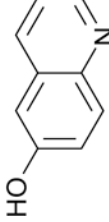
Compound	Structure	Ligand Efficiency (kcal mol ⁻¹ HA ⁻¹) PDE10A	K _i (μM), PDE10A	K _i (μM), PDE4A	X-ray; PDB ID
ZT0434 (18)		0.43	1300 ± 160	>2000	Y; 4LLX
ZT0429 (10)		0.43	300 ± 100	1800 ± 150	Y; 4MRZ
ZT0427 (9)		0.43	680 ± 370	1300 ± 160	N
ZT0214 (11)		0.42	380 ± 90	>2000	Y; 4LLJ
ZT0451 (7)		0.42	94 ± 24	460 ± 63	Y; 4MSN
ZT0449 (6)		0.37	500 ± 170	710 ± 64	Y; 4MSA
ZT0120 (b) (3)		0.37	500 ± 81	370 ± 29	Y; 4MRW
ZT0447 (c) (1)		0.37	550 ± 150	320 ± 27	N

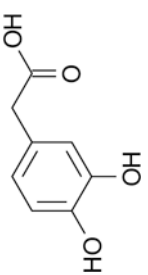
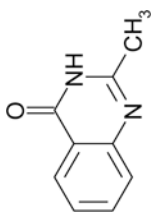

Compound	Structure	Ligand Efficiency (kcal mol ⁻¹ HA ⁻¹) PDE10A	K _i (μM), PDE10A	K _i (μM), PDE4A	X-ray; PDB ID
ZT0448 (c) (8)		0.36	560 ± 130	560 ± 43	Y; 4LM0
ZT0415 (15)		0.35	1400 ± 200	>2000	N
ZT0462 (14)		0.34	940 ± 200	1600 ± 97	Y; 4LM2
ZT0450 (19)		0.33	590 ± 180	K _{ic} = 170 ± 10 K _{int} = 670 ± 30	Y; 4LM1
ZT0464 (4)		0.30	1200 ± 280	810 ± 130	Y; 4LM3

Control compounds (IBMX, pentoxifylline, papaverine) are listed first, with fragments shown in LE order below the dashed line. Number in parenthesis corresponds to the position of the compound on the X-axis in Figure 1A. Average K_i values and the standard error of the mean are shown. Bold K_i values are those for which the K_i for PDE10A is different (p<0.05) than the K_i for PDE4A. Compounds were present at 2 mM in the final reaction, except as indicated: (a) 200 μM; (b) 0.5 mM; (c) 1 mM; (d) 20 μM. K_{ic}: competitive inhibition constant; K_{int}: uncompetitive inhibition constant. All values for PDE4A are from ¹³. X-ray indicates if high-resolution crystallographic data was obtained for the fragment bound to PDE10A.

Table 2

Inhibition Constants and Ligand Efficiencies of inhibitors of PDE10A

Compound	Structure	LE (kcal mol ⁻¹ HA ⁻¹)	#HA	K _i (μM)	X-ray; PDB ID
ZT0401 (NA)		0.68	9	16 ± 0.9 ^a	Y; 4LLP
ZT0017 (1)		0.41	11	450 ± 70	Y; 4LKO
ZT0419 (10)		0.39	11	700 ± 170	N
ZT0902 (25)		0.37	11	910 ± 270	Y; 4LM4
ZT0106 (44)		0.36	11	1200 ± 280	N

Compound	Structure	LE (kcal mol ⁻¹ HA ⁻¹)	#HA	K _f (μM)	X-ray; PDB ID
ZT0581 (66)		0.34	12	950 ± 530	N
ZT0217 (60)		0.34	12	990 ± 190	Y; 4LLK
ZT0826 (72)		0.29	13	1700 ± 300	N

Compounds Sorted Based on Ligand Efficiency (LE). Number in parenthesis corresponds to the position of the compound on the X-axis in Figure 1B. Average K_f values and the standard error of the mean are shown.

^a Determined using microcalorimetry. X-ray indicates if high-resolution crystallographic data was obtained for the fragment bound to PDE10A.